ISSN: 0067-2904

Enhancing the Signal-to-Noise Ratio of Astronomical Images with a Charge Injection Device

Raad Falih Hassan Foadi
Department of Astronomy and Space- College of Science- University of Baghdad, Baghdad, Iraq

Received: 2 /2/2024 Accepted: 16 /4 /2024 Published: 30 /4 /2025

Abstract

The signal-to-noise ratio of the Charge Injection Device is considered the most critical factor for evaluating the quality of the Charge Injection Device (CID). CID produces unwanted signals (noise) that can obscure the signal that needs to be detected. Noise is an essential obstacle for spectral identification of the observed object because it generates a fluctuation that can surpass the signal level. Therefore, reducing noise is very important to get a high-quality image. There are three main types of noise in the CID camera system: shot noise, readout noise, and dark current noise. The readout noise has the highest impact on the astronomical image because this noise is caused by a variety of factors, including trapping-state noise, reset noise, background noise, charge-transfer noise, and output amplifier noise. In order to reduce the readout noise and enhance SNR, non-destructive readout (NDRO) and binning techniques are used. This work examines the SNR of astronomical images with CID820 using NDRO, the binning process, and compound images. The study deals with three cases: the first is calculating SNR using different values of NDROs without binning. The second case uses different values of NDROs with 2, 4, and 6 binning. The third case involves combining two or more astronomical images to increase the SNR of CID820. Finally, the study compares the output results of SNR for the three cases to decide which case is the best for astronomical imaging using CID820.

Keywords: CID820, Signal-to-Noise Ratio, NDRO, Binning, Combining images.

تحسين نسبة الإشارة إلى الضوضاء للصور الفلكية المأخوذة بجهاز حقن الشحن

رعد فالح حسن فوادي

قسم علوم الفلك والفضاء ، كلية العلوم ، جامعة بغداد ، بغداد ، العراق

الخلاصه

نسبة الإشارة إلى الضوضاء (SNR) للصورة الماخوذة بجهاز حقن الشحن (CID) هي العامل الأكثر أهمية لتقييم جودة جهاز حقن الشحن CID. ينتج جهاز حقن الشحن إشارات غير مرغوب فيها (ضوضاء) التي يمكن أن تحجب الإشارة المراد الكشف عنها. تعد الضوضاء عقبة أساسية لتحديد الطيف للجرم المرصود لأنها تولد اشارة غير مرغوب بها يمكن أن يتجاوز مستوى اشارة الجرم. لذا، يعد تقليل الضوضاء أمرًا مهمًا للحصول على صورة عالية الجودة. هناك ثلاثة أنواع رئيسية من الضوضاء في نظام جهاز حقن الشحن، وهي:

*Email: Raad.n@sc.uobaghdad.edu.iq

blooming. Therefore, CCD devices are unsuitable for an Extreme Contrast Ratio (ECR) imager device. The charge injection device (CID820) is suitable for being considered the prime imager for ECR in astronomy. The CID820 features inherent anti-blooming, non-destructive readouts that reduce readout noise and a high dynamic range equal to 10^9 [1]. Readout noise occurs during the process of converting charge carriers into a voltage signal and the following process of converting the analog-to-digital (A/D). The on-chip preamplifier typically contributes the most to readout noise, and this noise is distributed uniformly to each image pixel. Some kinds of noise in the Charge Transfer Device's (CTD's) output amplifier are frequency-dependent. The readout noise has a bad influence on the signal-to-noise level, which affects image quality. This work will examine the non-destructive readout, binning processes, and combined images to determine if they enhance the signal-to-noise ratio in an astronomical image and the best value for each. Section 2 depicts the theoretical component, which includes CID, noise types, SNR, and NDRO. Section 3 illustrates image reduction, binning images, and combined images. Section 4 presents the results and discussions. Section 5 concludes with some findings.

1. Theoretical Part

2.1 Charge Injection Device (CID):

The Charge Injection Device (CID) is a semiconductor device that supports random pixel addressing and binning. It has a sizeable full-well capacity (235,000 electrons). It is radiation-resistant. The active pixel array has dimensions of 2048H*2048V and a pixel area of 12µm*12µm. Due to its front illumination, this sensor has a quantum efficiency of 48% at 525nm. Each pixel has a fill factor of 60% [2, 3].

2.2. Noise:

The noise in imaging sensors was classified into two types according to their production: temporal noise and spatial noise. The temporal noise is produced in the sensor's pixel during the signal collection process. This type of noise is time-dependent noise, such as shot noise, flicker noise (1/f), and thermal noise (dark current noise). The spatial noise is caused by the sensor’s system design, which considers space-dependent noise such as fixed pattern noise (FPN) [4].

2.2.1. The photon-shot noise :

It is caused by the random influx of photons that reaches the detector. It all depends on how the photon behaves. At high illumination, photon-shot noise is responsible for most of the noise. This implies that the photon-shot noise is proportional to the intensity of the flux hitting the detector [5, 6, 7].

2.2.2. Flicker noise:

Flicker noise, often known as 1/f noise, is caused by crystal imperfections and defects that form charge carrier traps. The traps collect and release charge carriers randomly, so they cause carrier numbers to fluctuate. Flicker noise can be reduced by employing Correlated Double Sampling (CDS) [8].

2.2.3. Thermal noise:

Thermal noise (Johnson noise) is created by random electron mobility. Thermal effects in the resistive regions cause random motion. Thermal noise is affected by temperature and conductor resistance. The thermal noise's power spectral density is given by

$$n_{th} = 4kTR \quad (1)$$

T is the absolute temperature; k is Boltzmann's constant; and R is the resistance [5, 6].

2.2.4 Fixed Pattern Noise (FPN):

It is a type of noise that is space-dependence. The differences in the transistors across the sensor generate FPN. FPN increases with light exposure; however, it impacts image quality more at low illumination. This type of noise has three sources: dark current and non-uniformity. The second source is the pixel source, which results from the difference in transistor voltage thresholds between the pixels. The third source is the column source, created by fluctuation in column amplifiers, where the gain of the amplifier and analog to digital converters (ADC) varies from column to column [6, 7].

2.3. Signal to Noise Ratio (SNR):

It is an important ratio to evaluate image quality. SNR is the ratio of the signal's power to the power of noise at a particular signal level in a specific system. It is given by:

$$SNR = 20\log_{10}\frac{N_{signal}}{N_{noise}} \text{ (dB)} \quad (2)$$

N_{signal} is the number of electrons in the signal, and N_{noise} is the number of electrons in the noise. The noise dominates the SNR at low illumination, and the dominating noise is dark current noise. Because the dark current noise in the system is constant, the SNR grows linearly with increasing flux intensity. When the degree of illumination increases, shot noise takes over, which is represented by the square root of the signal electrons, and the equation above becomes [9]:

$$SNR = 20\log_{10}\frac{N_{signal}}{N_{noise}} = 20\log_{10}\sqrt{N_{signal}} \quad (3)$$

The greatest value of SNR that can be achieved is at the saturation level. Increasing SNR is dependent on increasing the full-well capacities of the imager's pixel and reducing floor noise [9, 10]

2.4 Non-Destructive Readout (NDRO)

This process allows the pixel to be read as often as necessary before the stored charge is applied to the substrate. The CID820 can do 2, 4, 8, 16, 32, 64, 128, and 256 non-destructive readouts. Figure 1 (a-c) shows the process of the NDRO method [11,12, and 13]. Figure 2 shows how the readout noise decreases with the number of NDROs, from 45 e- for one NDRO to 5.8 e- for 128 NDRO.

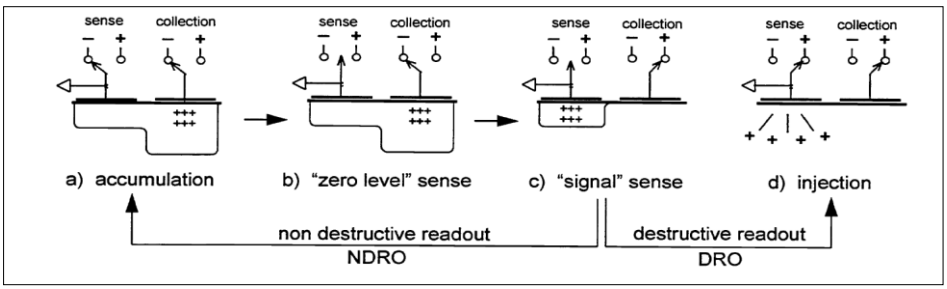

Figure 1: Photon collection and the readout scheme of a single CID pixel [12]

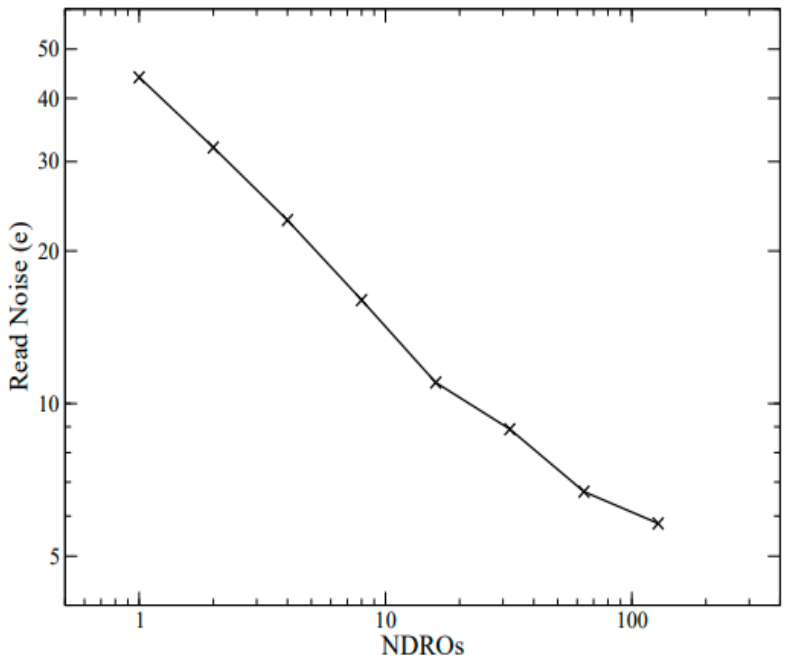

Figure 2 SXDR read noise vs. number of NDROs (N). The lowest read noise is 5.8 e^- RMS for N = 128. [14]

3. Practical Part

3.1 Observations

The observations were conducted in March 2015 at the Cassegrain 0.8 m reflector telescope equipped with a CID820 camera at Ortega Observatory, Melbourne, Florida. The array size is 2048 × 2048 pixels, providing an image scale of 0.6 arcsec/pixel.

3.2 Data Reduction

The calibration of the astronomical image was applied to calculate the SNR. First, remove the dark current by subtracting the dark current frame from the raw image. Second, the flat field frame is used to remove the defects in the image that occur because of the dust and the optics effect. These processes will be explained in this section.

3.2.1 Dark Current

According to the Fermi-Dirac distribution, when silicon is heated above absolute zero, thermal electrons are collected in a pixel's potential well. As a result, even without a light source, a detector will capture a signal (thermal electrons). The 'dark current' is defined as the number of thermal electrons created per second per pixel. The dark current value varies from pixel to pixel depending on pixel sensitivity. Some pixels are overheated due to an excessive number of thermal charge carriers. The dark current is a temperature-dependent and time-dependent mechanism [15, 16].

Dark current can be reduced using the cooler, ethylene glycol for the CID820, mixed 50:50 with DI water. The CID820 achieved -45.1 C, resulting in a dark current of 0.3 electrons per second per pixel. The additional signal caused by the dark current should be subtracted from the CID820 image. A separate frame containing only the dark current signal should be obtained. This was accomplished by taking an exposure at the same time as the CID820's image but keeping the CID820 shutter closed to guarantee that no light enters the CID820 sensor. As a result, the only signal captured is the thermal electron. The dark current frame must be removed. To eliminate the influence of thermal electrons from the original signal (source

signal), the dark current frame must be subtracted from each CID820 image. The dark current frame was produced using ten frames for 200 seconds and took their median [9].

$$R(i,j) = I(i,j) - \left(\frac{\sum_{i=1}^{N} D(i,j)}{N*Time}\right) * Exposure\ time \quad (4)$$

$$R(i,j) = I(i,j) - \left(\frac{D(i,j)}{200}\right) * Exposure\ time \quad (5)$$

Where *R(imj)* is the new frame after subtracting the dark current noise from the raw frame, *I(I,j)* represents the raw frame, the term $\frac{\sum_{i=1}^{N} D(i,j)}{N*Time}$ refers to the sum of the dark current frames divided by the total time they were imagining them, and *exposure time* is the imaging time of the astronomical object.

3.2.2 Flat Field Frame

The flat field frame should be used to remove the effect of dust on the telescope's mirrors or lenses, optical distraction, and different imagers' pixel sensitivity to light. The pixel-to-pixel response function of CID820 images was determined using twilight flats at sunset. Ten frames were taken at different times. These frames were normalized, and their median or average was used to produce the final flat field frame. The raw astronomical image R will be divided by the flat field frame (F) [17].

$$F(i,j) = \frac{1}{10}\left(\sum_{i=1}^{N}\sum_{j=1}^{N}\sum_{m=1}^{10} f(i,j,m)\right) \quad (6)$$

$$S(i,j) = R(i,j)/F(i,j) \quad (7)$$

3.3 Binning image

It is to join many adjacent pixels into one region that can be read simultaneously. On the one hand, this gives the advantage of a higher readout frequency and a better signal-to-noise ratio, but on the other hand, it reduces resolution [18]. The pixels in the CID camera are not physically joined but are read out collectively. In this work, the binning process was done using the MATLAB program.

3.4 Combine images:

It was used to add two or more images to each other to form one final astronomical image. Individual images have a certain level of signal electrons to noise electrons. When combining these images, the signal electrons' level to the noise's electrons is increased, which leads to an increase in the SNR. Combining images can be described as follows: The first step is doing the image collaboration for each image. The second step is choosing reference points in each astronomical image to collect the signal from the same source in the same pixel in the final image. The last step is forming a new astronomical image from the added images.

4- Results and discussion

Figure (3) shows how the SNR is increased using the NDRO, where 4, 8, 16, 32, 64, 128, and 256 NDRO were used. The 256 NDRO gave a better result but consumed more time than the other NDRO processes; therefore, it is unsuitable for fast astronomical imaging.

The binning process is enhancing SNR. However, increasing the binning number from 2 to 6 decreases the resolution from 0.02 arcseconds per pixel to 0.0065 arcseconds per pixel and may result in pixelation. The binning process in this work was done using MATLAB programming. Figure (4) shows the NDRO and Binning 2×2, 4×4, and 6×6. In order to calculate the resolution of an astronomical image, the following formula is used [9]:

Resolution = (206.265 * Pixel Size) / Focal Length (8)

Focal length = aperture *focal ratio (9)

Where: Pixel Size is the size of each pixel in micrometers; Focal Length is the telescope's focal length in millimeters; therefore, the resolution will be in arcseconds per pixel.

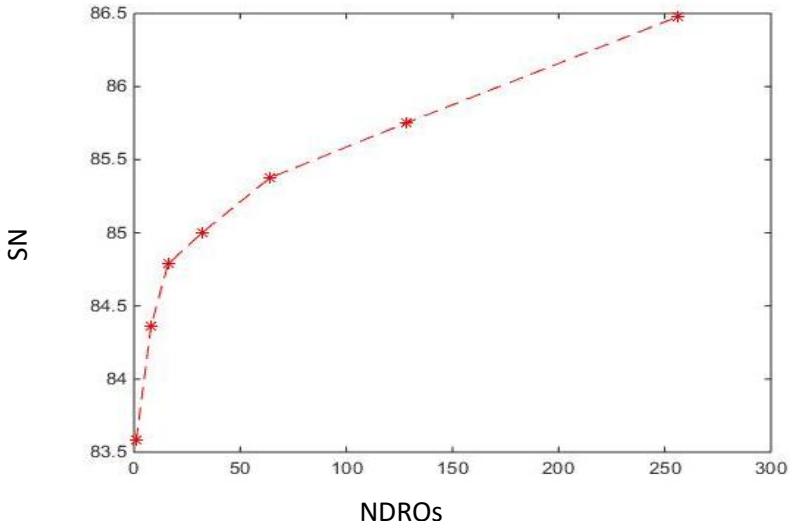

Figure 3: Shows the SNR of astronomical image as a function of NDRO without binning for Sirius with exposure time 20s.

The resolution of an image after binning can be calculated using the following formula [9], as shown in Table 1:

New Resolution = Original Resolution / Binning Factor (10)

Table 1: The resolution after the binning process was applied to the astronomical image

Binning factor	Resolution (arcsec/pixel)
1×1	0.0387
2×2	0.01935
4×4	0.00967
6×6	0.00645

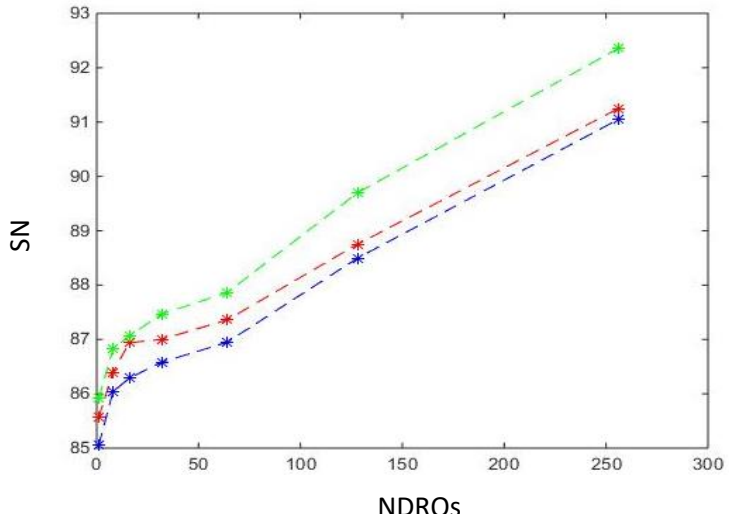

Figure (4) Shows the SNR of an astronomical image as a function of NDRO with different binning values. The green line represents SNR with 2×2 binning, the red line represents SNR with 4×4 binning, and the blue line represents SNR with 6×6 binning. (Sirius with 20s exposure time)

Table 2 shows the result of combining three images with NDRO 64, 128, and 256, respectively. The first row shows the SNRs without binning for the images 85.3627, 85.7503, and 86.4765. The SNR after combining the images was 91.1715. The second row shows the SNRs with a binning of 2×2 for the three images: 87.8627, 89.6973, and 92.3561. After combining the images, the SNR was 98.7490.

Table 2: The result of combining three images with NDRO 64, 128, and 256, respectively.

Image number	Image1 (NDRO 64)	Image 2 (NDRO 128)	Image 3 (NDRO 256)	Combined Image
(Without binning)	85.3761	85.7503	86.4765	91.1715
SNR (With binning 2×2)	87.8627	89.6973	92.3561	98.7490

5- Conclusion:

In summary, different methods have been used in this work to enhance the astronomical image's SNR with CID. Three methods are investigated: NDRO, the binning process, and combining images. As described in this work, the methods are used separately and together to see how the value of SNR is affected. The signal-to-noise ratio value is enhanced by using different values of NDRO, as shown in Figure (3) because the read noise is reduced with increasing NDRO numbers, as shown in Figure (2). Applying the binning with NDRO increases the SNR for the astronomical image, as shown in Figure (4). However, the binning process reduces the resolution of the image. Therefore, to keep a better resolution while enhancing SNR, the 2×2 binning is used based on the result in Table 1. The value of the SNR of an astronomical image is optimized using the combined images method, as illustrated in Table 2. When the three methods are used together, the SNR is enhanced from 83.5 (in case NDRO = 1, and without using binning or combining image methods) to 98.74.

References:

[1] S. M. Sawant and D. Batcheldor, "Charge-injection Device Imaging of Sirius with Contrast Ratios Greater than 1: 26 Million," Publications of the Astronomical Society of the Pacific, vol. 134, no. 1033, pp. 034503, 2022.

[2] S. Bhaskaran, T. Chapman, M. Pilon, and S. VanGorden "Performance based CID imaging: past, present, and future," in Infrared Systems and Photoelectronic Technology III, vol. 7055, SPIE, 2008.

[3] Thermo Fisher Scientific Inc., "Thermo Scientific SpectraCAM XDR™," 2007.

[4] S. Xie and A. J. P. Theuwissen, "Suppression of spatial and temporal noise in a CMOS image sensor," IEEE Sensors Journal, vol. 20, no. 1, pp. 162-170, 2019.

[5] K. T. Tian, W. O. Bearden, and G. L. Hunter, "Consumers' need for uniqueness: Scale development and validation," Journal of Consumer Research, vol. 28, no. 1, pp. 50-66, 2001.

[6] J. Nakamura "Image sensors and signal processing for digital still cameras," CRC Press, 2005.

[7] X. Wang, P. R. Rao, and A. J. P. Theuwissen, "Fixed-pattern noise induced by transmission gate in pinned 4T CMOS image sensor pixels," in 2006 European Solid-State Device Research Conference, pp. 331-334, IEEE, 2006.

[8] A. Michailidis, T. Noulis, and K. Siozios, "CMOS Noise Analysis and Simulation from Low Frequency and Baseband to RF and millimeter Wave," IEEE Access, 2023.

[9] R. Foadi, Extreme Contrast Ratio Imaging with Charge Injection Devices, Florida Institute of Technology, 2015.

[10] N. H. Resham, H. K. Abbas, H. J. Mohamad, and A. H. Al-Saleh, "Noise Reduction, Enhancement and Classification for Sonar Images," Iraqi Journal of Science, vol. 62, no. 11, pp. 4439–4452, Dec. 2021.

[11] S. Bhaskaran, M. Pilon, B. Pirger, S. VanGorden, and J. Zhang, "Linear CID sensor array with on-chip analog memory for time-resolved scientific applications," in Detectors and Imaging Devices: Infrared, Focal Plane, Single Photon, vol. 7780, pp. 227-237, SPIE, 2010.

[12] B. S. Backer, Z. Ninkov, and M. Corba, "Characterization of a CID-38 charge injection device," in Solid State Sensor Arrays and CCD Cameras, vol. 2654, pp. 11-19, SPIE, 1996.

[13] D. Darson, J. Dubois, M. Bourdernane, B. Heyrman, P. Morfin, A. Douiyek, and D. Ginhac, "Real-time high dynamic range based on multiple nondestructive readout during a single exposure: application to IR imaging," in Proceedings of the 11th International Conference on Distributed Smart Cameras, pp. 21-28, 2017.

[14] D. Batcheldor, R. Foadi, C. Bahr, J. Jenne, Z. Ninkov, S. Bhaskaran, and T. Chapman, "Extreme Contrast Ratio Imaging of Sirius with a Charge Injection Device," Publications of the Astronomical Society of the Pacific, vol. 128, no. 960, pp. 025001, 2016.

[15] S. B. Howell, Handbook of CCD astronomy, Cambridge University Press, 2006.

[16] G. E. Healey and R. Kondepudy, "Radiometric CCD camera calibration and noise estimation," IEEE Transactions on Pattern Analysis and Machine Intelligence, vol. 16, no. 3, pp. 267-276, March 1994.

[17] F. R. Chromey, To measure the sky: an introduction to observational astronomy, Cambridge University Press, 2010.

[18] J. Egberts, "Investigations on transverse beam profile measurements with high dynamic range," Ph.D dissertation, Ruprecht-Karls Universität Heidelberg, 2009.